Chapter 9

Micro/Nano Liquid Crystal Layer–Based Tunable Optical Fiber Interferometers

Haimei Luo, Changjing Wang, Yinghua Ji and Wen Yuan

Additional information is available at the end of the chapter

http://dx.doi.org/10.5772/intechopen.70413

Abstract

Miniaturization and integration are the main trends in modern photonic technology. In this chapter, two kinds of micro-/nano liquid crystal (LC) layer–based tunable optical fiber interferometers are proposed. One fiber interferometer is the optical fiber gratings (LPGs), and the other one is the locally bent microfiber taper (LBMT). The working principles of the devices are theoretically analyzed. The preparation process and the functional properties of the devices are experimentally investigated as well.

Keywords: liquid crystal device, fiber gratings, microfiber taper, interferometry, mode

1. Introduction

As optical materials that exhibit very large anisotropic properties, liquid crystal (LC) has been used in a variety of photonic applications with an eye toward enabling tunable optical responses, with stimuli including thermal [1], electrical [2], magnetic [3], and optical fields [4]. Miniaturization and integration are the main trends in modern photonic technology. With the help of micro-/nanofabrication technology, people can design and prepare various optical fiber micro-/nanostructures and devices, which exhibit significant difference in characteristics when the functional structure size decreases to micrometers and/or nanometers. These special physical properties have wide theoretical research prospects and practical applications. In this chapter, two kinds of novel micro-/nano LC layer–based tunable optical fiber interferometers are theoretically analyzed and experimentally studied, including the mode coupling properties and relevant micro-/nanofabrication technologies. The operation principle, preparation process, and functional properties of the proposed optical fiber devices are studied in detail. By comparison

with that of the traditional sized optical fiber devices, the advantages in performance of the micro-/nano LC layer based ones are verified. The main contents of this chapter are as follows.

Two kinds of typical optical fiber–based modal interference devices and the relevant micro-/nanofabrication technology are proposed in Section 2.1. One typical fiber modal interference device is the optical fiber grating. The other typical device is the tapered optical fiber. Adopting optic fiber surface micro-/nanostructure technology, two kinds of micro-/nano liquid crystal layer–based wide range tunable optical fiber devices are achieved. The properties of the cladding modes in LPG coated with a high refractive index (HRI) micro-/nanometer overlay are theoretically studied in Section 2.2. The resonant wavelength and spectral characteristics of the four layer model long period grating are also analyzed based on the coupled-mode theory. Besides, the transmission spectra of LPG with different overlay thickness and refractive indices are numerically calculated. The tuning characteristics of locally bent microfiber taper (LBMT) covered with a nanosized HRI layer under different temperatures and electric field intensities have been theoretically analyzed in Section 2.3. The mathematical model for LBMT is established. The mode coupling and interference characteristics in a LBMT are described. In Section 2.4, a new structure LPG coated with nanosized HRI-LC layer is experimentally realized. The refractive indices of LC at different temperatures are measured. Using the sample brush coating technology, LC layers with different thicknesses are deposited on the surface of LPG. The sensitivity of the resonance wavelength to the change of the nanoscale overlay refractive index is experimentally observed. Experimental results show that the phenomenon of cladding mode reorganization in HRI-LC–coated LPG occurs when the high refractive index (HRI) of the nanosized LC overlay is changed from 1.477 to 1.515 resulting from temperature increasing from 20 to 65°C. The electro-optic tuning ability of LPG coated with the HRI-LC layer is also demonstrated. By choosing an appropriate operating point, the maximum tuning range can reach approximately 10 nm. The experimental results are in good agreement with the theoretical analysis in Section 2.2. The transmission characteristics of the nanosized HRI-LC layer–coated LBMT in response to the environmental temperature, and external electric fields have been experimentally investigated in Section 2.5. A microfiber taper with a diameter of ~3.72 μm is fabricated using the flame brushing technique. By bending the transition region of the taper and later by placing a ~200-nm LC layer over the uniform taper waist region, a high-efficiency thermal and electric tunable LC-coated LBMT interferometer is achieved. This suggests a potential application of this device as tunable all-fiber photonic devices, such as filters, modulators, and sensing elements. Finally, conclusions are drawn in section 3.

2. Micro-/nano LC layer–based tunable optical fiber interferometers

2.1. Two kinds of typical optical modal interferometers

2.1.1. Long period gratings (LPG)

In-fiber long period gratings (LPG), which have the ability to couple energy from the code mode to different cladding modes with the same propagation direction, have been widely investigated in the field of optical sensing and communication [5].

http://dx.doi.org/10.5772/intechopen.70413

Up to date, most of the studies have concentrated on the analysis of the LPG response to the surrounding medium refractive index (SRI) smaller than that of silica [6]. The idea of coated LPG with a thin HRI layer was first put forward by Rees et al. [7]. Then, Wang et al. presented a detailed study to investigate the sensitivity of LPG to SRI when they are coated with a nano-sized HRI film [8]. In the same year, a comprehensive investigation of mode transition in HRI layer–coated LPG was reported by Cusano et al. [9]. Their analysis indicated that the cladding modes reorganization occurred for a fixed overlay thickness and refractive index by increasing the SRI. In fact, changing the HRI could also result in cladding modes reorganization. The theoretical and experimental study proposed by Del Villar et al. showed that by selecting an appropriate overlay thickness, the highest sensitivity of the resonance wavelengths to HRI change of the overlay can be obtained [10, 11].

2.1.2. Tapered optical fiber interferometer

Fiber tapers, which have a variety of functions including filtering, light coupling, and sensing, consist of a waist between two tapered sections fabricated by heating and pulling technology [12, 13]. Different length and shape of the first tapered section have different effects on the input mode [13].

Recently, we reported a compact fiber interferometer named LBMT interferometer [14–16]. This kind of interferometer has unique features of low insertion loss and ultrathin taper waist, so it is promising for high-sensitivity sensing. It is interesting to integrating a LBMT interferometer and functional material due to physical effect of functional material and the high sensitivity of the microfiber to the surroundings.

2.2. Mode transition in the nanosized HRI overlay–coated LPG

2.2.1. Theory background

Based on the phase-matching condition between the core and the cladding modes, the center wavelength λ_i of the *j*th attenuation band can be expressed as [17]

$$\lambda_i = \left(n_{co} - n_{cl}^i\right)\Lambda \tag{1}$$

where n_{co} is the effective refractive index of the core mode and n_{cl}^i is the effective refractive index of the *i*th cladding mode. Λ is the grating period [5].

Figure 1 shows the structure of HRI-coated LPG with four layers. Using the transfer matrix method proposed by Anemogiannis et al., the cladding mode effective index can be calculated [18].

2.2.2. Numerical analysis of HRI overlay–coated LPG

The analysis used the standard Corning SMF-28 optical fiber parameters: numerical aperture 0.14, refractive index difference 0.36% [9], cladding, and core diameter 125 and 8.2 μm, respectively. The HRI-LC overlay is with refractive index of 1.47–1.55 close to the experimental testing [19] and with different thickness changing from 600 to 900 nm.

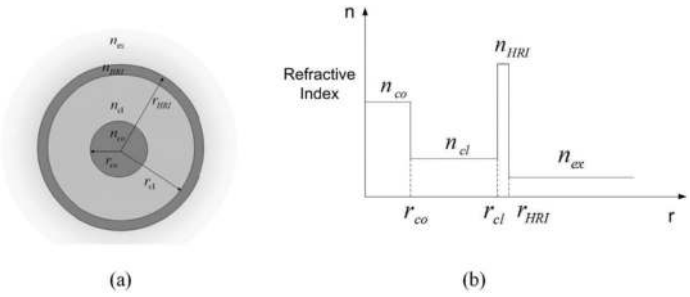

Figure 1. (a) Illustrative schematic of LPG with an nm-thick thin-film coating. (b) Index profile of the thin-film coated LPG.

Each effective refractive index of the first six cladding modes as a function of the HRI is represented in **Figure 2(a)** for a 600-nm HRI overlay. From the figure, we know that each effective refractive index of the first six cladding modes goes up as the HRI increases, until a critical point is reached, when a significant shift in the effective refractive index occurs. There is a specific value of HRI that makes the lowest order cladding mode to be guided within the overlay for a fixed overlay thickness.

Figures 2(b)–(d) show the effective refractive index for a HRI overlay of 700, 800, and 900 nm, respectively. It can be seen that the transition point moves to a lower HRI as the overlay thickness increases.

2.3. Tuning effect of nanosized HRI-LC overlay–coated LBMTs

2.3.1. Mode coupling and interference in LBMTs

The fiber taper can be divided into two zones: (1) the taper waist with a constant diameter d_0 and (2) the transition region with a diameter continuously varying from d_0 to 125 μm. A LBMT is fabricated by bending the transition regions of the taper to form a modal interferometer.

To study the modal characteristics in the bent transition region, we assume the bent fiber taper as a sequence of straight segments of the same length l with an angle of θ [20] (see **Figure 3(a)**) [15]. The complex amplitude, $a_{pq}^{(i+1)}$, of the modes in the (i+1)th region is given by [20]

$$a_{pq}^{(i+1)} = \sum_{n=0}\sum_{m=0} \int_0^{\infty}\int_0^{2\pi} \Psi_{nm}^{i} \exp\left(-j\beta_{nm}^{i} l^{i}\right) \times \exp\left(j\beta_{nm}^{i}\theta r\cos\varnothing\right)\Psi_{nm}^{(i+1)*} r dr d\varnothing, \mathrm{i} = 1, 2, \ldots \quad (2)$$

where l^i is the length of the ith region, β_{nm}^{i} and ψ_{nm}^{i} are the propagation constant and the normal field of the LP_{mn} mode in the ith region, respectively [15]. $\psi_{pq}^{(i+1)*}$ is the complex conjugate of the mode field of the LP_{pq} mode in the (i+1)th region [15].

The local-mode power evolution along the LBMT under various bending curvatures was theoretically examined. The LBMT parameters are as follows: d_0 = 3.7 μm, L_0 = 6 mm, and

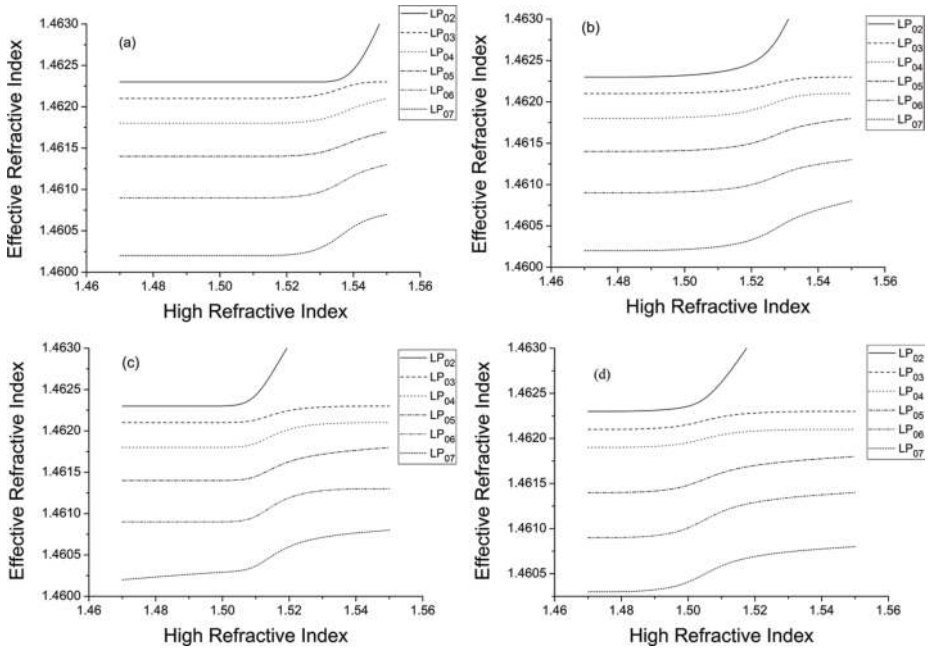

Figure 2. Effective refractive index of the LP_{02} – LP_{07} cladding modes versus HRI-coated fiber with (a) 600, (b) 700, (c) 800, and (d) 900 nm film.

L_t = 3 mm at λ = 1.550 μm. Each bent transition region was divided into 100 steps with the same length (L_t/M). The 6-mm long uniform waist region has been considered as a step. From the modal shown in **Figure 3(b)** [15], we can calculate the appropriate values of the angle θ in the bent transition region. **Figure 4** shows the evolution of the first four modes (LP_{01}, LP_{11}, LP_{21}, and LP_{02}). As we can see that there is no power transfer from the fundamental mode to other high-order modes when the bending curvature 1/R = 0. As the bending curvature goes up, the LP_{11}, LP_{21}, and LP_{02} modes are successively excited with their energy originated from the LP_{01} mode. The power of each mode remains almost constant in the central uniform taper waist. When 1/R increases, the coupling between the fundamental mode and the first higher order mode, the decisive factor in the interference extinction ratio is strengthened. The optimized status can be obtained at a certain bending curvature (e.g. 0.455 mm^{-1}) with the maximum extinction ratio and the relatively low loss.

2.3.2. Spectral tuning characteristics of a LBMT with a nanosized HRI-LC overlay

We calculated Poynting vectors of 200-nm LC layer–coated silica microfiber with different diameters ranging from 1 to 5 μm operating at 1.55 μm wavelength by solving Maxwell's equations of a three-layer structured cylindrical wavelength numerically (see **Figure 5(a)–(c)**)

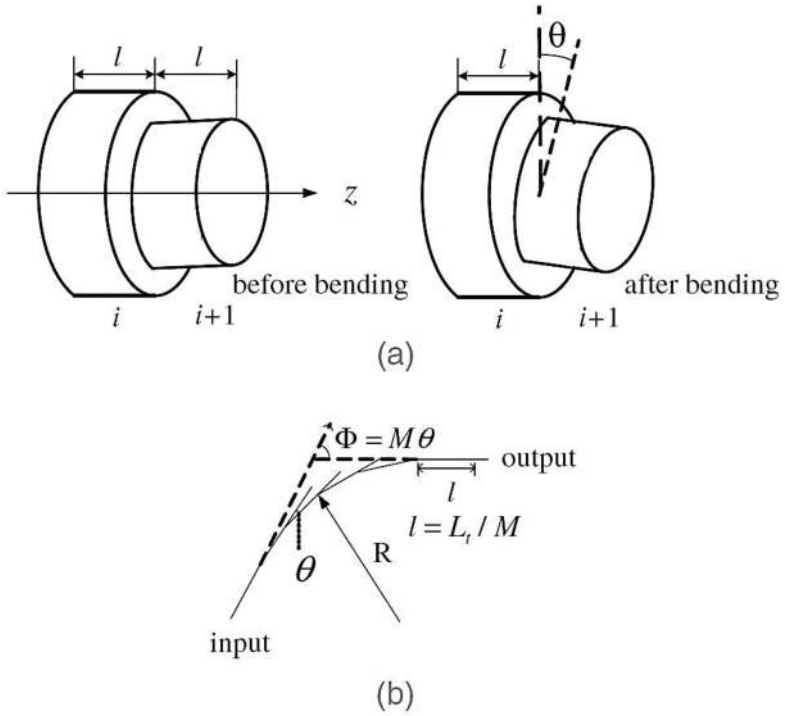

Figure 3. (a) Two adjacent sections of a fiber before and after bending. (b) Geometry used for the theoretical analysis of the bending effect on the fiber taper [15].

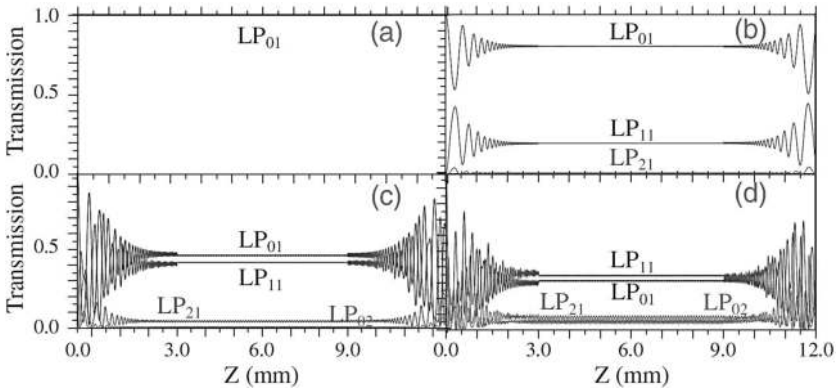

Figure 4. LP_{nm} local-mode power longitudinal evolution of the LBMT with d_0 = 3.7 μm and L_0 = 6 mm under bending curvature $1/R$ being (a) 0, (b) 0.2, (c) 0.445, and (d) 0.526 mm^{-1} at λ = 1.555 μm.

http://dx.doi.org/10.5772/intechopen.70413

[16, 21]. In our calculation, the refractive indices of LC and silica microfiber are 1.50 and 1.44, respectively. We also calculated the amount of optical power guided in the LC layer and the air as a function of microfiber diameter in **Figure 5(d)** and **(e)**, respectively [16]. When the diameter of microfiber goes up from 1 to 5 μm, the amount of optical power is changed from 18.4 to 0.98% in the LC layer and from 10.5 to 0.31% in the air, respectively, which results in smaller tuning efficiency and lower transmission loss.

High-order modes are excited successively from the fundamental mode after the light injects into the uniform taper waist from a locally bent transmission region. In the output bent transition region, these modes will couple back into the fundamental mode and the wavelength-dependent transmission spectrum could be expressed as [16]

$$I = \sum_m I_m + 2\sum_{m>n}\sum \sqrt{I_m I_n}\cos\left(2\pi\Delta n_{eff} L_0/\lambda\right) \tag{3}$$

where I_m is the amplitude of the propagation mode, Δn_{eff} is the effective index difference, and L_0 is the length of the taper waist. The attenuation peak wavelength λ_N of the interferometer can be expressed as [16]

$$\lambda_N = 2\Delta n_{eff} L_0/(2N+1) \tag{4}$$

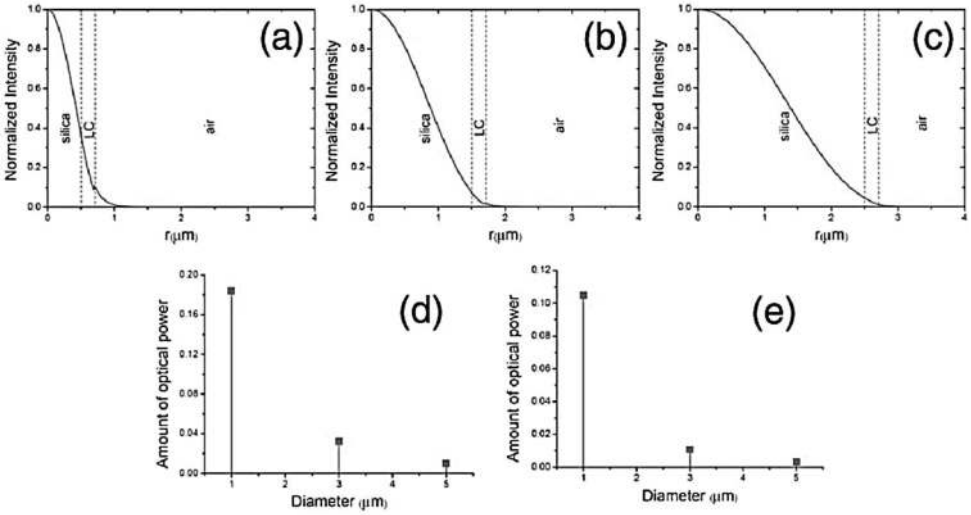

Figure 5. Calculated Poynting vector of a 200-nm thick LC-coated microfiber with diameter being (a) 1, (b) 3, and (c) 5 μm. The amount of optical power guided in (d) LC overlay, and (e) air as a function of microfiber diameter [16].

where N is the interference order. According to Eq. (4), Δn_{eff} changes when the effective index of the propagation mode of the microfiber taper waist is altered by the surrounding refractive index, and as a result, a wavelength shift is obtained. **Figure 6** shows the calculated Poynting vectors of a 3.72-μm diameter silica microfiber coated with different thickness HRI-LC overlay when wavelength is at 1.55 μm. As we can see, thicker LC films assure more optical power guided in the overlay for the fundamental mode and the first high-order mode. More optical power is converted to the radiation mode when the overlay thickness increases, which will result in a higher transmission loss.

The calculated transversal mode distributions for the first two modes with different 200-nm LC overlay HRIs are plotted in **Figure 7**. **Figure 8** depicts the effective index difference Δn_{eff} of the fundamental mode and the first high-order mode as a function of the refractive index of LC, when the overlay thickness being 200, 400, and 600 nm. We can see that more light energy concentrates in the outside LC layer with higher refractive index of the LC overlay, leading to an increased tuning range. The microfiber taper interferometer with higher overlay refractive index or thicker overlay thickness exhibits higher sensitivity. The higher the refractive index of the overlay, the smaller the effective index difference Δn_{eff}.

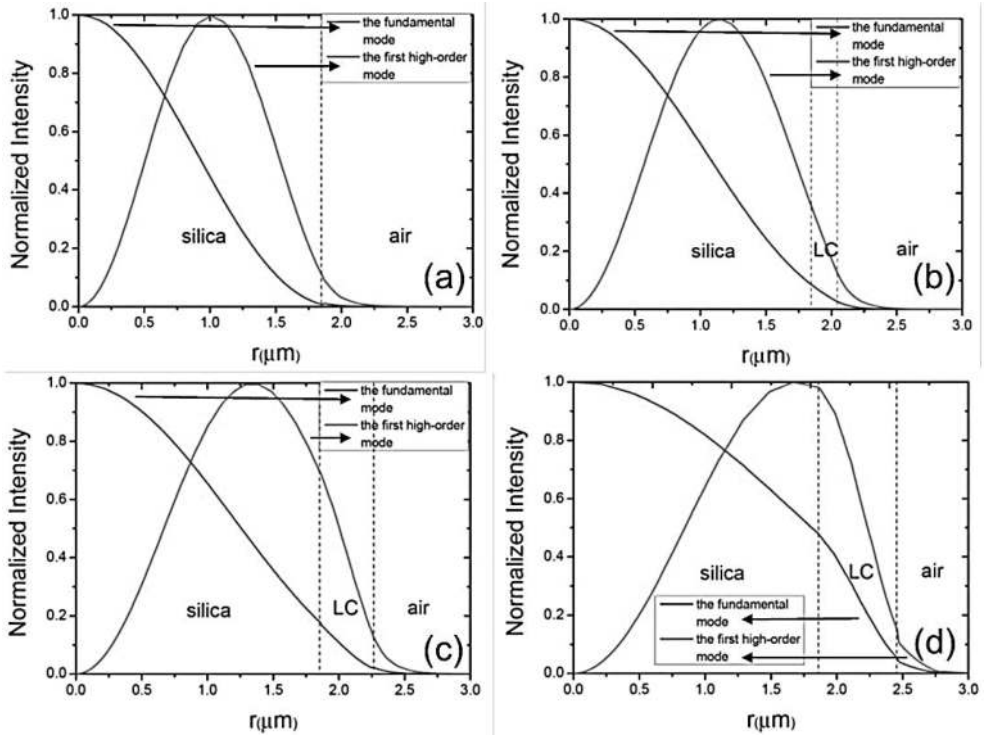

Figure 6. Distribution of the fundamental mode and the first high-order mode for three LC overlay thickness values: (a) 0, (b) 200, (c) 400, and (d) 600 nm.

http://dx.doi.org/10.5772/intechopen.70413

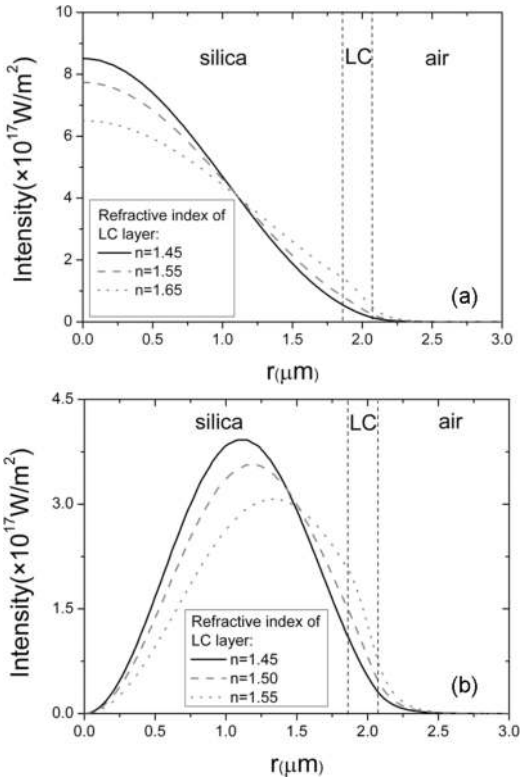

Figure 7. Transversal electric field distributions of the fundamental mode and the first high-order mode guided in the microfiber taper waist coated with a 200 nm LC overlay. (a) The fundamental mode and (b) the first high-order mode.

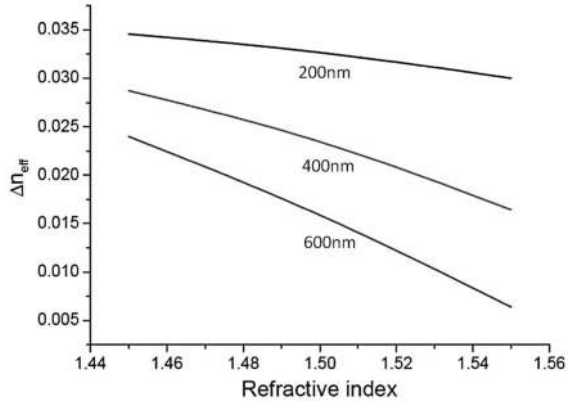

Figure 8. Calculated dependence of Δn_{eff} on the refractive index and the thickness of the LC overlay at the wavelength of 1559 nm.

2.4. Experimental study of nanosized HRI-LC layer–coated LPG

2.4.1. Temperature-dependent mode transition in HRI-LC–coated LPG

The LPG was fabricated on Corning SMF-28 fibers through CO_2 irradiation. The grating period is 620 μm, and the grating region is 50 mm. A white light source and an optical spectrum analyzer are used to record the spectral response. Attention bands were focus on the LP_{02} and LP_{03} modes in the range of 1400–1700 nm.

LC material MDA-98-3699 is from Merck. The refractive index of LC is higher than that of silica. The coating process is simple. We dipped a tampon with the liquid crystal, and daubed it on the fiber grating evenly. The surface tension of the slimy liquid crystal makes itself uniformly coated. **Figure 9** shows the CCD photographs of the bare and LC-coated LPG taken by

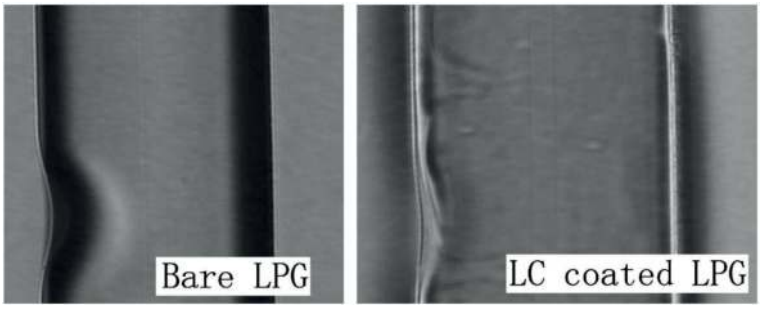

Figure 9. CCD photographs of bare and LC-coated LPG.

OLYMPUS STM6 measuring microscope. The thickness of the LC layer is controlled by the times of daubing. **Figure 10** shows the CCD photographs of overlay thickness of about (a) 400 and (b) 800 nm. A heater box was used to change the temperature of the liquid crystal from 20 to 65°C.

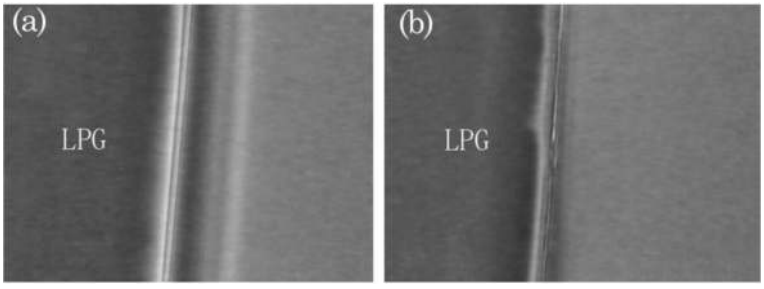

Figure 10. CCD photographs reveal approximate overlay thicknesses of (a) 400 and (b) 800 nm.

http://dx.doi.org/10.5772/intechopen.70413

Figure 11 shows the transmission spectrum of the ultrathin LC-coated LPG for different temperatures between 20 and 65°C. From the figure, we know that when temperature is increased from 20 to 58°C, wavelength blueshifts slightly (the LP_{0i} mode has been marked with *i*). A large wavelength shift is obtained in the attenuation band of LP_{03} mode when the temperature goes up to about 59°C. The phenomenon of cladding modes reconfiguration appears when temperature in changed from 58 to 60°C.

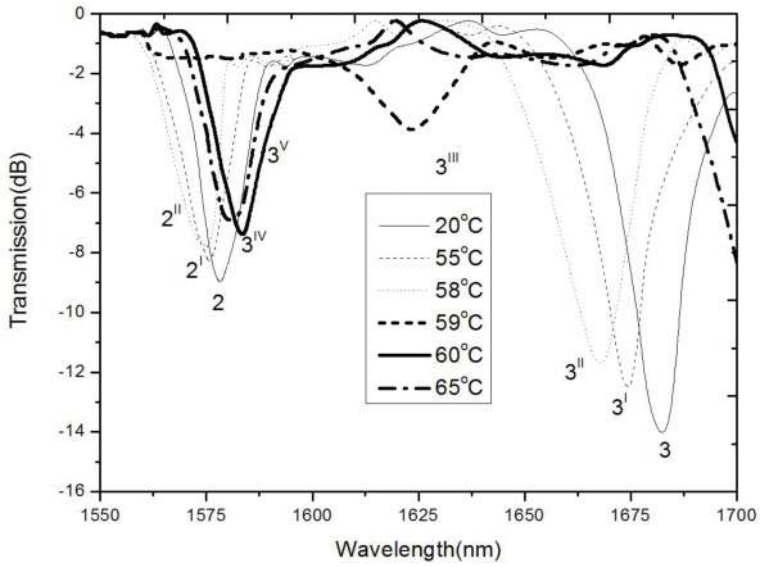

Figure 11. Transmission spectra of an ultrathin HRI-LC–coated LPG for different temperatures in the 20–65°C range.

Figure 12 shows a clearer wavelength shift. As we can see, outside the transition region, the center wavelength of the LP_{02} mode shifts from 1579.7 to 1579.2 nm, and the LP_{03} mode shifts from 1687.5 to 1665.7 nm. However, only LP_{03} mode can be observed within the transition region with its center wavelength changing from 1665.7 to 1583.7 nm, which shifts ~82 nm.

2.4.2. Measurement of the refractive index of LC at different temperatures

To clarify the experimental observations, the temperature dependent refractive index of the LC overlay was also measured. The methods for measuring the refractive index of liquids can be classified into refraction technique and reflection techniques including total reflection [22]. **Figure 13** shows the schematic diagram of the experiment setup with an efficient method developed by Pu et al. [23].

We immerse a detecting tip into air, water, and LC under different magnetic fields. The reflected light power under every condition is measured. **Figure 14** shows the thermo-dependent HRI of LC in the infrared light region based on the experimental data.

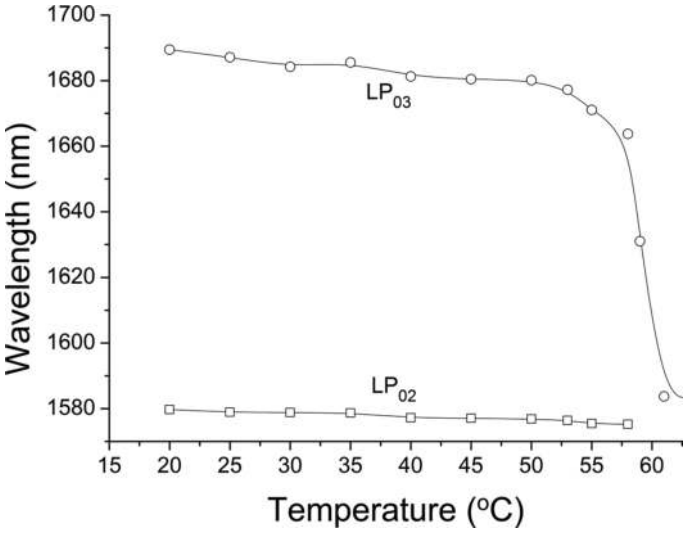

Figure 12. Wavelength shift of LP_{02} and LP_{03} cladding modes for the LPG coated with a HRI layer versus temperature.

Figure 15 shows the theoretically calculated center wavelength shifts with the measured HRI data. The experimental results are in good agreement with the theoretical analysis. For LP_{03} mode, the sensitivity to HRI in the transition region was approximately six times the sensitivity outside the transition region, which means that we can choose this region as high-sensitivity operating region for sensing application.

2.4.3. Electrical spectral tuning of LC-coated LPG at the highly sensitive operating point

A simple scheme for active electrically controlled tunable fiber gratings is illustrated schematically in **Figure 16**. Two parallel substrates are used to fix the LC-coated LPG separated by two 125-μm spacers. The external electric fields are applied through a pair of electrodes under stabilized temperature at 20, 55, 58, 59, 60, and 65°C. The electrical spectra tunability of the LC-coated LPG under different temperatures is shown in **Figure 17**. As we can see that the most sensitive operating point for the device is at 60°C, the maximum tuning range is about 10 nm.

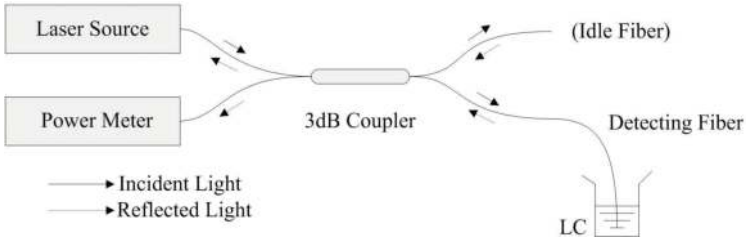

Figure 13. Schematic diagram of experimental setup for measuring the refractive index of the LC.

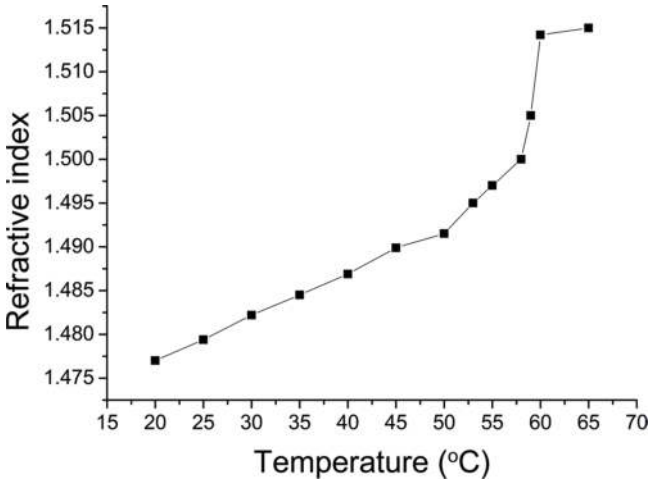

Figure 14. Refractive index versus temperature (°C) of LC MDA-98-3699.

2.5. Experimental investigation of nanosized LC-coated LBMT interferometer

Figure 18 shows the experimental setup. The microfiber taper integrated with the nanosized LC layer was pulled straightly first, and then, the transition regions of the microfiber taper were locally bent to form a fiber interferometer. Two pieces of strip electrodes parallel to each other were pressed against the microfiber with a 4-μm gap maintained by spacers. The profile parameters of the microfiber taper are as follows: the waist diameter $d_0 \approx 3.72$ μm, waist length $L_0 \approx 6.3$ mm, and bent transition region length $Lt \approx 3$ mm. These parameters are given in **Figure 18(b)** together with the critical diameter corresponding to the bent transition region. **Figure 18(c)** shows the SEM image of the taper waist.

The LC material MDA-98-3699 is from Merck [16, 24]. CCD photographs of the bare and LC-coated microfiber taper waist are shown in **Figure 19**. By rubbing the strip electrodes directly on both sides of the microfiber, the planar anchoring of the LC can be obtained.

A comparison of transmitted spectra of a bare and LC-coated LBMT interferometer at 25°C is given in **Figure 20**. Compared with the bare one, a redshift of ~4.9 nm and a decrease of the transmission loss peak of ~2 dB can be observed.

We first measured the transmission spectra of the bare microfiber interferometer at temperatures ranging from 25 to 50°C, and the temperature responses for the attenuation peak at the wavelength of 1529.3 nm are shown in **Figure 21**. Here, we can see from **Figure 21** that the temperature response is only 0.026 nm/°C.

As to thermal tuning, we use the temperature dependence of the ordinary effective index of LC. We measured the ordinary refractive indices of the LC under different temperatures at a wavelength of 1.55 μm [25]. The ordinary refractive index of the LC increases linearly from 1.4794 to 1.4845 when the temperature goes up from 25 to 35°C.

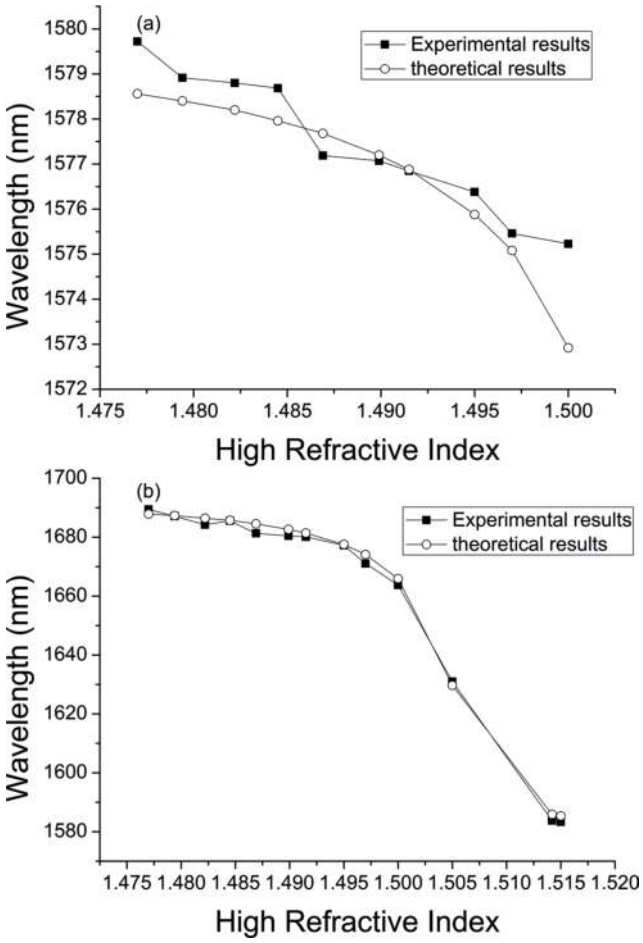

Figure 15. Theoretical and experimental center wavelength of (a) LP_{02} and (b) LP_{03} shift dependence on HRI.

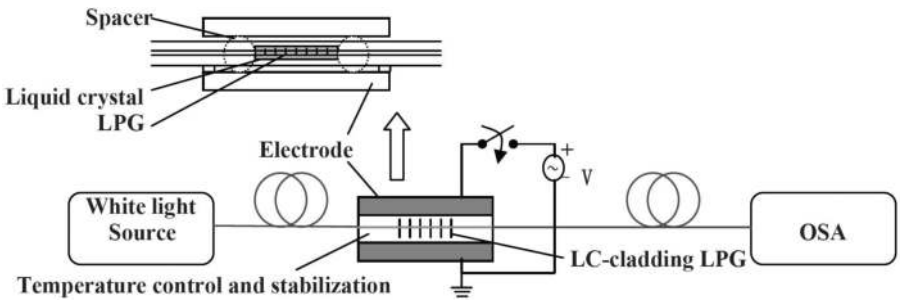

Figure 16. Experimental setup and schematic representation of the LC cladding LPG.

http://dx.doi.org/10.5772/intechopen.70413

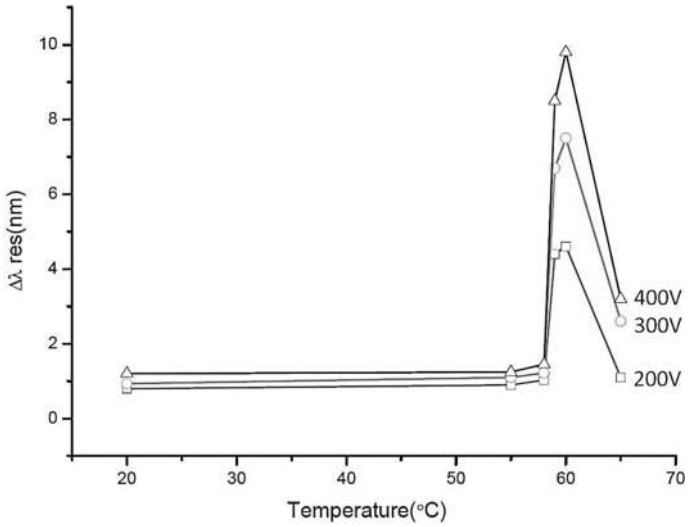

Figure 17. Electrical spectra tenability of the LC cladding LPG at different temperatures.

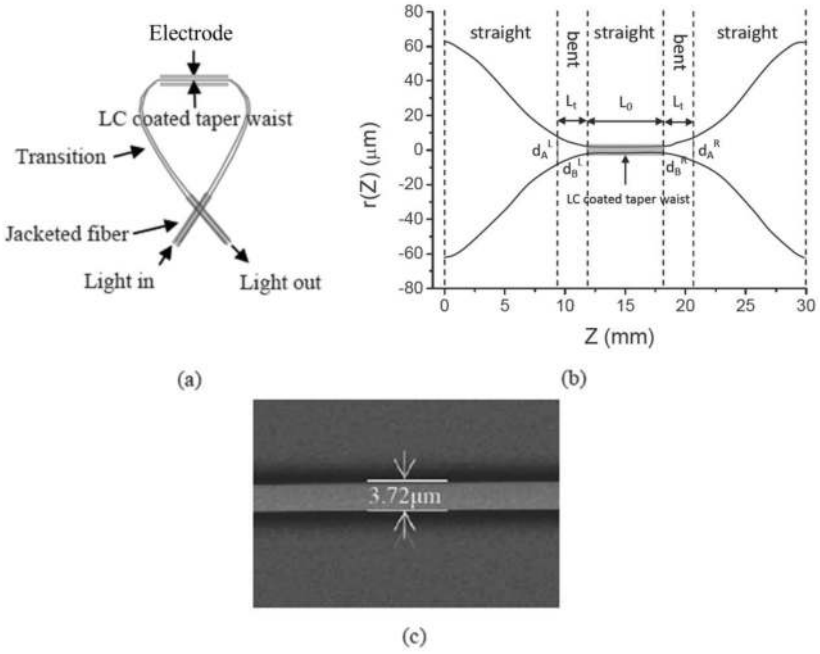

Figure 18. (a) Schematic diagram of the experimental setup for magnetic field tenability test; (b) measured profile of the LBMT having $d_0 \approx 3.72$ μm, $L_0 \approx 6.3$ mm with d_A and d_B corresponding to the bent transition region; (c) SEM image of the microfiber taper waist with a diameter of ~3.72 μm.

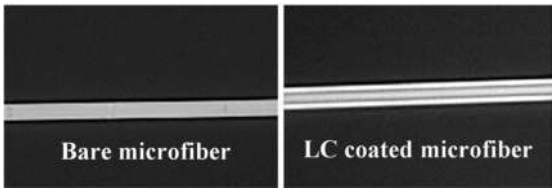

Figure 19. CCD photographs of bare and LC-coated microfiber taper waist.

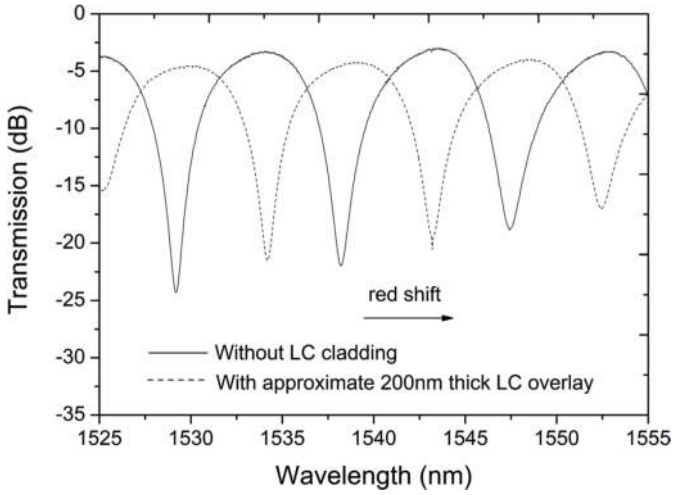

Figure 20. Comparison of the transmission spectra of a bare and an approximate 200 nm LC-coated LBMT interferometer.

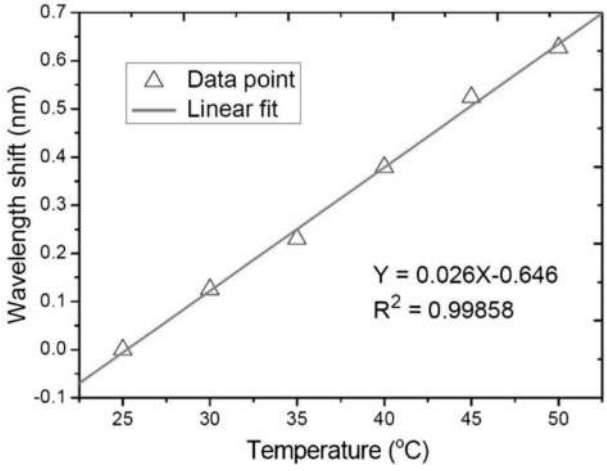

Figure 21. Temperature responses of bare microfiber interferometer for the attenuation peak at the wavelength of 1529.3 nm.

A redshift of 10.5 nm for the attenuation peak wavelength of 1534.2 nm was achieved as temperature increased from 25 to 35°C, as shown in **Figure 22**. The tuning efficiency is ~1.05 nm/°C, which is approximately 40 times higher than that of the bare locally bent microfiber interferometer.

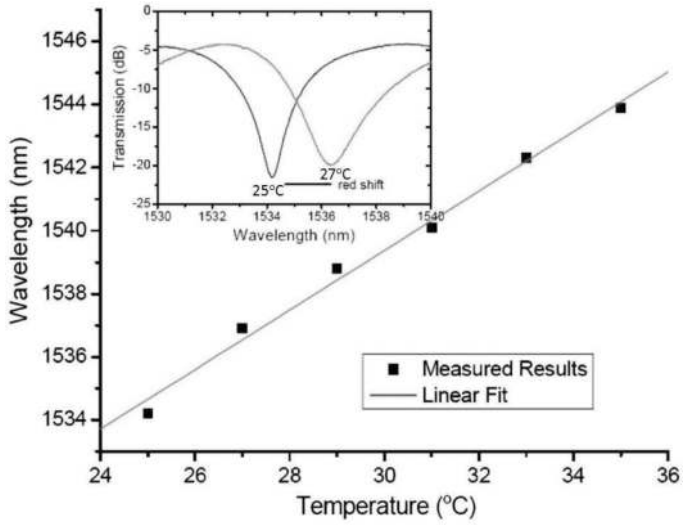

Figure 22. Measured wavelength shifts of a certain attenuation peak of the interferometer at different temperatures.

As to electric tuning, electric fields of 1.25, 2.50, and 3.75 V/μm were applied to the electrodes in our experiment by adjusting the tunable voltage source with the temperature stabilized at 25°C [16]. **Figure 23(a)** is the measured transmission spectra of the same attenuation peak under different electric fields. **Figure 23(b)** is the wavelength of attenuation peak as a function

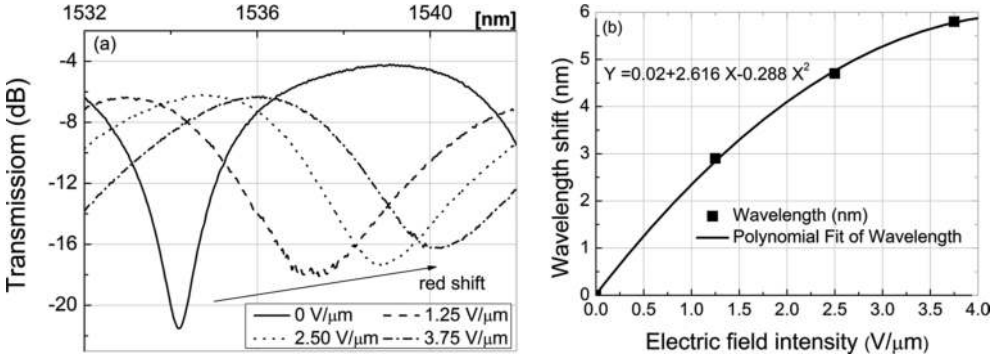

Figure 23. (a) Transmission spectra of LC-coated LBMT interferometer according to the external electric field and (b) wavelength shift of the transmission spectrum with the variation of the electric field intensity.

of the electric field. From the figures, we can see that the wavelength dip experiences some redshift by ~5.8 nm, when the electric field changes from 1.25 to 3.75 V/μm. Due to the uniaxial birefringent properties, the optic axis of nematic LC can be realigned by electric field. The effective refractive index is given by $n_{\text{eff}} = 1/\sqrt{(\cos^2\theta/n_0^2)^2 + (\sin^2\theta/n_e^2)^2}$, when the light polarization direction has an angle θ with respect to the average alignment of the molecules [19]. These experimental results are in good accordance with the above theoretical analysis.

3. Conclusions

In this chapter, two kinds of micro/nano LC layer based tunable optical fiber interferometers are reported. For interferometer 1, experimental results show that shifts of greater than 80 nm in the attenuation bands of the transmission spectrum of LPG can be obtained by changing the refractive index of the LC overlay through the thermo-optic effect. For interferometer 2, due to the high sensitivity of the microfiber taper waist to the LC overlay refractive index, the thermal sensitivity as high as 1.05 nm/°C has been achieved, and the electrical tuning range is ~ 5.8 nm when the external electric field is applied up to 3.75 V/μm. The results suggest that the potential application of the micro/nano LC layer based fiber interferometers as tunable all-fiber photonic devices, such as filter and all-optical switch.

Acknowledgements

This work was supported in part by National Science Foundation of China (NSFC) (51567011, 11264016, 61505073, 61363012); China Scholarship Council (CSC) (201608360081); Science and Technology Project of Jiangxi Province (20151BDH80060, 20151BBG70062, 20161ACB21011, 20161BAB212045); Project of Jiangxi Province Department (160273, 150313).

Author details

Haimei Luo*, Changjing Wang, Yinghua Ji and Wen Yuan

*Address all correspondence to: nclhm2002@hotmail.com

Jiangxi Normal University, Nanchang, Jiangxi, China

References

[1] Hu DJJ, Shum P, Lu C, Sun X, Ren GB, Yu X, Wang GH. Design and analysis of thermally tunable liquid crystal filled hybrid photonic crystal fiber coupler. Optics Communications. 2009;**282**(12):2343-2347. DOI: 10.1016/j.optcom.2009.03.023

[2] Song L, Lee WK, Wang XS. AC electric field assisted photo-induced high efficiency orientational diffractive grating in nematic liquid crystals. Optics Express. 2006;**14**(6):2197-2202. DOI: 10.1364/OE.14.002197

[3] Zyryanov VY, Myslivets SA, Gunyakov VA, Parshin AM, Arkhipkin VG, Shabanov VF, Lee W. Magnetic-field tunable defect modes in a photonic-crystal cell. Optics Express. 2010;**18**(2):1283-1288. DOI: 10.1364/OE.18.001283

[4] Chen Z, Hsiao VKS, Li XQ, Li Z, Yu JH, Zhang J. Optically tunable microfiber-knot resonator. Optics Express. 2011;**19**(15):14217-14222. DOI: 10.1364/OE.19.014217

[5] Luo HM, Wang CJ, Wang XP, Wang YF, Yuan W. The effects of the nanosized high refractive index overlay on tunable long period gratings with normal and reduced cladding diameters. Optik. 2016;**127**:5230-5234. DOI: 10.1016/j.ijleo.2016.02.083

[6] Patrick HJ, Kersey AD, Bucholtz F. Analysis of the response of long period fiber gratings to external index of refraction fraction. Journal of Lightwave Technology. 1998;**16**(9): 1606-1612.

[7] Rees ND, James SW, Tatam RP, Ashwell GJ. Optical fiber long-period gratings with Langmuir–Blodgett thin-film overlays. Optics Letters. 2002;**27**(9):686-688. DOI: 10.1364/OL.27.000686

[8] Wang Z, Heflin JR, Stolen RH, Ramachandran S. Analysis of optical response of long period fiber gratings to nm-thick thin-film coatings. Optics Express. 2005;**13**(8):2808-2813. DOI: 10.1364/OPEX.13.002808

[9] Cusano A, Iadicicco A, Pilla P, Contessa L, Campopiano S, Cutolo A. Mode transition in high refractive index coated long period gratings. Optics Express. 2006;**14**(1):19-34. DOI: 10.1364/OPEX.14.000019

[10] Del Villar I, Matias IR, Arregui FJ. Long-period fiber gratings with overlay of variable refractive index. IEEE Photonics Technology Letters. 2005;**17**(9):1893-1895. DOI: 10.1109/LPT.2005.853283

[11] Del Villar I, Corres JM, Achaerandio M, Arregui FJ, Matias IR. Spectral evolution with incremental nanocoating of long period fiber gratings. Optics Express. 2006;**14**(25):11972-11981. DOI: 10.1364/OE.14.011972

[12] Goure JP, Verrier I. Optical Fibre Devices. 1st ed. London: CRC Press; 2010. 269 p.

[13] Mas S, Marti J, Palaci J. Curvature investigation in tapered fibers and its application to sensing and mode conversion. Optics and Lasers in Engineering. 2015;**74**:109-113. DOI: 10.1016/j.optlaseng.2015.05.011

[14] Luo HM, Li XW, Zou WW, Li X, Hong ZH, Chen JP. Temperature-insensitive microdisplacement sensor based on locally bent microfiber taper modal interferometer. IEEE Photonics Journal. 2012;**4**(2):772-778. DOI: 10.1109/JPHOT.2012.2197606

[15] Luo HM, Li XW, Zou WW, Jiang WN, Chen JP. Modal interferometer based on a C-shaped ultrathin fiber taper for high-sensitivity refractive index measurement. Applied Physics Express. 2012;**5**:012502. DOI: 10.1143/APEX.5.012502

[16] Luo HM, Wang CJ, Ji YH, Yuan W, Zhang GP, Wang YF, Hong ZH. Spectral tuning of a locally bent microfiber taper interferometer with a nanosized liquid crystal overlay. Applied Optics. 2016;**55**(26):7393-7397. DOI: 10.1364/AO.55.007393

[17] Vengsarkar AM, Lemaire PJ, Judkins JB, Bhatia V, Erdogan T, Sipe JE. Long-period fiber gratings as band-rejection filters. Journal of Lightwave Technology. 1996;**14**(1):58-65. DOI: 10.1109/50.476137

[18] Anemogiannis E, Glysisv EN, Gaylord TK. Transmission characteristics of long-period fiber gratings having arbitrary azimuthal/radial refractive index variation. Journal of Lightwave Technology. 2003;**21**(1):218-227. DOI: 10.1109/JLT.2003.808637

[19] Luo HM, Li XW, Wang SS, Chen JP. Temperature stabilized electrically tunable long period gratings coated with nanosized liquid crystal layer. In: Optical Society of America, editor. OFC/NFOEC; 22-26 March 2009; San Diego, CA, USA. IEEE. 2009. p. JThA22

[20] Shankar PM, Bobb LC, Krumboltz HD. Coupling of modes in bent biconically tapered single-mode fibers. Journal of Lightwave Technology. 1991;**9**(7):832-837. DOI: 10.1109/50.85782

[21] Lou JY, Tong LM, Ye ZZ. Dispersion shifts in optical nanowires with thin dielectric coatings. Optics Express. 2006;**14**(16):6993-6998. DOI: 10.1364/OE.14.006993

[22] Schmid K and Penzkofer A. Refractive-index measurements with a Pellin-Broca prism apparatus. Applied Optics. 1983;**22**(12):1824-1827. DOI: 10.1364/AO.22.001824

[23] Pu S, Chen X, Chen Y, Liao W, Chen L, Xia Y. Measurement of the refractive index of a magnetic fluid by the retroreflection on the fiber-optic end face. Applied Physics Letters. 2005;**86**:171904. DOI: 10.1063/1.1905808

[24] Luo HM, Li XW, Li SG, Chen JP. Analysis of temperature-dependent mode transition in nanosized liquid crystal layer-coated long period gratings. Applied Optics. 2009; **48**(25):F95-F100. DOI: 10.1364/AO.48.000F95

[25] Yin SZ, Chung KW, Zhu X. A highly sensitive long period grating based tunable filter using a unique double-cladding layer structure. Optics Communications. 2001;**188** (5-6):301-305. DOI: 10.1016/S0030-4018(00)01172-X